This is a repository copy of *Magnetic-silk/polyethyleneimine core-shell nanoparticles for targeted gene delivery into human breast cancer cells*.

White Rose Research Online URL for this paper:
http://eprints.whiterose.ac.uk/139857/

Version: Published Version
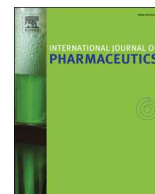
Magnetic-silk/polyethyleneimine core-shell nanoparticles for targeted gene delivery into human breast cancer cells

Wenxing Song[a,b], David A. Gregory[a], Haider Al-janabi[c], Munitta Muthana[c], Zhiqiang Cai[b], Xiubo Zhao[a,b,*]

[a] Department of Chemical and Biological Engineering, University of Sheffield, Sheffield S1 3JD, UK
[b] School of Pharmaceutical Engineering and Life Science, Changzhou University, Changzhou 213164, China
[c] Department of Infection and Immunity, University of Sheffield, Sheffield S10 2RX, UK

ABSTRACT

The lack of efficient and cost-effective methods for gene delivery has significantly hindered the applications of gene therapy. In this paper, a simple one step and cost effective salting-out method has been explored to fabricate silk-PEI nanoparticles (SPPs) and magnetic-silk/PEI core-shell nanoparticles (MSPPs) for targeted delivery of c-myc antisense oligodeoxynucleotides (ODNs) into MDA-MB-231 breast cancer cells. The size and zeta potential of the particles were controlled by adjusting the amount of silk fibroin in particle synthesis. Lower surface charges and reduced cytotoxicity were achieved for MSPPs compared with PEI coated magnetic nanoparticles (MPPs). Both SPPs and MSPPs were capable of delivering the ODNs into MDA-MB-231 cells and significantly inhibited the cell growth. Through magnetofection, high ODN uptake efficiencies (over 70%) were achieved within 20 min using MSPPs as carriers, exhibiting a significantly enhanced uptake effect compared to the same carriers via non-magnetofection. Both SPPs and MSPPs exhibited a significantly higher inhibition effect against MDA-MB-231 breast cancer cells compared to human dermal fibroblast (HDF) cells. Targeted ODN delivery was achieved using MSPPs with the help of a magnet, making them promising candidates for targeted gene therapy applications.

1. Introduction

Gene therapy has shown great potential for the treatment of many diseases (Zhao et al., 2007; Zhang et al., 2014; Zhang et al., 2016). Efficient gene therapy requires the delivery of genes to the cell nucleus or cytoplasm replacing or regulating the defective genes (Zhang et al., 2014). However, several intracellular barriers such as the cell membrane and endosome membrane have significantly reduced its efficiency (De Smedt et al., 2005; Pack et al., 2005). Therefore, carriers are needed to help the gene delivery (Zhang et al., 2014). Efficient and cost-effective carriers are particularly desired for clinical applications.

Due to the potential toxicity and immunogenicity concerns of viral systems (El-Aneed, 2004; Plank et al., 2003; Lungwitz et al., 2005), non-viral gene delivery systems have been explored as an alternative method for gene therapy (Lungwitz et al., 2005; Zhang et al., 2014;

Zhang et al., 2016). The advantages of non-viral systems include low cost, ease of fabrication and modification, and high *in vivo* stability (Zhang et al., 2016). One of the most efficient and cost-effective agents is polyethyleneimine (PEI) (Lungwitz et al., 2005; Dey et al., 2011; Xiang et al., 2007; Forrest et al., 2003; Seow et al., 2013). Once mixed with DNAs, PEI is able to condense DNAs into nano complexes that are suitable for the cell internalization through endocytosis (Zhang et al., 2014; Wang et al., 2009). In addition, PEI is able to destabilize the endosomal membrane by the 'proton sponge effect' to protect DNAs against degradation and facilitate the release of DNAs from endosomes into cytoplasm (Zhang et al., 2014; Wang et al., 2009; Dey et al., 2011; Xiang et al., 2007). Despite its high transfection efficiency, the applications of PEI are still limited by its inherent problems such as high cytotoxicity and lack of targeting (Forrest et al., 2003). Attempts have been made to improve targeting by developing PEI coated magnetic

nanoparticles (MPPs) for gene delivery through magnetofection (Zhang et al., 2014; Zhang et al., 2016), in which an external magnetic field was used to enhance the transfection efficiencies by rapidly concentrating the magnetic vectors on the cell surface (Huth et al., 2004).

However, MPPs still possess significant cytotoxic effects and lead to a decreased viability to many cell lines (Hoskins et al., 2012; Hoskins et al., 2012; Strojan et al., 2017; Du et al., 2016). Hoskins et al. (2012) investigated this by exposing MCF-7, SH-SY5Y and U937 cells to 100 μg/ml of MPPs and observed cell viability decreased to 50%, 70% and 80% respectively after a 24 h incubation. When the incubation time was increased to 7 days, the cell viability of these cells decreased to 20%, 10%, and 30% respectively (Hoskins et al., 2012). To further reduce the cytotoxicity of MPPs, various approaches have been investigated (Hoskins et al., 2012; Hoskins et al., 2012; Strojan et al., 2017; Du et al., 2016). Hoskins et al. (2012) reported that MCF-7, SH-SY5Y and U937 cells exhibited viabilities over 95% after 24 h incubating with MPPs-PEG and around 90% after 7 days. Strojan et al. (2017) fabricated glutathione modified PEI coated magnetic nanoparticles (GSH NPs) by adding glutathione during nanoparticle synthesis and reported that glutathione reduced 30% cytotoxic effects to CHO cells. Another example is reported by Du et al. (2016), where PEI was modified with lactose at different lactosylation degrees (6.8% and 11.7%) and then coated onto magnetic nanoparticles (MNPs). The resulting lactose modified MPPs showed reduced cytotoxicity to RAW 264.7 cells compared with unmodified MPPs. However, the above particles have limited manipulation of the size and zeta potential. Only the GSH NPs have been used for gene delivery test and the efficiency was compromised (Strojan et al., 2017).

In this work, a simple one-step salting-out method has been explored to fabricate silk-PEI nanoparticles (SPPs) and magnetic-silk/PEI core-shell nanoparticles (MSPPs) for targeted delivery of c-myc antisense oligodeoxynucleotides (ODNs) into MDA-MB-231 breast cancer cells. Silk fibroin (SF) protein from cocoons of *Bombyx mori* is an FDA approved, natural material which has been widely used to form various biomaterials including gels, sponges and films for different medical applications such as drug delivery, tissue engineering and wound dressing (Vepari and Kaplan, 2007). Excellent biocompatibility (Dal Pra et al., 2005), tuneable biodegradability (Horan et al., 2005) and easy processing (Vepari and Kaplan, 2007) of SF has made it a promising biomaterial for drug and gene delivery systems (Vepari and Kaplan, 2007; Liu et al., 2014; Yu et al., 2016; Li et al., 2014; Mathur and Gupta, 2010). However, the fabrication of magnetic-silk/PEI core-shell nanoparticles (MSPPs) and their performance as gene delivery carriers has not yet been reported. Here, SF was used to help the particle formation through salting-out and manipulate the size and zeta potential of the nanoparticles, as well as reduce the cytotoxicity of MPPs. The morphology, size and zeta potential of the nanoparticles and their ODN complexes were determined by DLS, AFM and TEM. Toxicity of nanoparticles with different SF percentages and the cell growth inhibition effects using their ODN complexes against MDA-MB-231 cells and HDF cells were determined through the MTT assay. The cell uptake profiles and the localization of nanoparticle-ODN complexes were investigated by flow cytometry and confocal microscopy. The results show that the MSPPs were efficient carriers for ODN delivery, therefore they are promising candidates for targeted delivery of ODNs into cancer cells.

2. Materials and methods

2.1. Materials

Na$_2$HPO$_4$ (S7907), NaH$_2$PO$_4$ (S8282), ammonium hydroxide (221228), DMSO (Dimethyl sulfoxide, D5879), branched polyethyleneimine (408727) were purchased from SIGMA-ALDRICH. *Bombyx mori* silk was obtained from Jiangsu, P.R. China. Single-stranded human c-myc antisense oligodeoxynucleotides (5′-AAC-GTT-GAG-GGG-CAT-3′, with and without 5′-FAM (carboxyfluorescein-5-

succimidyl ester) labelled) were purchased from Eurogentec Ltd. (UK) and were HPLC purified. Iron (II) chloride tetrahydrate (44939), Iron (III) chloride hexahydrate (44944), Oligofectamine (12252011), Alexa Fluor® 568 phalloidin (A12380), MTT (M6494), foetal bovine serum (FBS, 10500064) and DAPI (4′, 6-Diamidino-2-phenylindole dihydrochloride, D1306) were purchased from Thermo Fisher Scientific. MDA-MB-231 cells (Human Caucasian Breast Adenocarcinoma cells) were purchased from ECACC. HDF cells were provided by the Sheffield RNAi screening facility. RPMI (Roswell Park Memorial Institute) 1640 Medium (BE 12-167F), PBS (Dulbecco's Phosphate Buffered Saline, BE17-512F), L-glutamine (17-605F) were purchased from Lonza®.

2.2. Preparation of silk fibroin solution

Silk fibroin (SF) solutions were prepared based on the protocol previously reported (Song et al., 2017). Briefly, silk fibres were boiled for 30 min in 0.02 M Na$_2$CO$_3$ solution and then rinsed 3 times with DI water to remove sericin (this step is also called degumming). The degummed SF was dried overnight in a drying oven at 60 °C before added into a ternary system (CaCl$_2$/Ethanol/water at molar ratio of 1:2:8) and heated to keep the system temperature at 75 °C for 3 h with stirring. The solid SF was dissolved in the solution within 30 min. The SF solution was dialysed in a cellulose dialysis tube (12.5 KDa molecular weight cut off) against DI water for 3 days, during which the DI water was replaced at least 5 times per day. The resulting solution was centrifuged twice at 10,000g for 10 min to remove the impurities before stored at 4 °C.

2.3. Preparation of magnetic nanoparticles (MNPs)

Iron (III) chloride hexahydrate (4 g) and iron (II) chloride tetrahydrate (4.5 g) were each dissolved in 150 ml DI water and degassed with nitrogen for 30 min to remove the oxygen in the solutions. The solutions were then mixed in a 500 ml round-bottom flask and 15 ml of ammonium hydroxide was added under vigorous stirring in a nitrogen atmosphere at room temperature for 2 h. The magnetic nanoparticles (MNPs) were collected with strong Neodymium magnets and washed at least 5 times with DI water to remove any impurity. The particles were then washed with ethanol and dried over night at room temperature and stored for future usage.

2.4. Preparation of SPPs and MSPPs

2.4.1. Preparation of SPPs

SF solution (5 mg/ml) and PEI solution (5 mg/ml) were mixed at different volume ratios (10:90, 25:75, 50:50, 75:25 and 90:10) to prepare SF/PEI mixtures. 2 ml of SF/PEI mixtures were then added to 10 ml of sodium phosphate solutions (Na$_2$HPO$_4$ + NaH$_2$PO$_4$) with an ionic strength of 1.25 M at pH 8. The prepared solutions were kept at room temperature (20 °C) for 6 h to allow the formation of particles. The resultant solution was then centrifuged at 20,000g for 15 min to collect the SPPs. The particles were washed several times with DI water to remove excess salts before further characterizations. SF and PEI particles were prepared using the same method as controls.

2.4.2. Preparation of MSPPs

MNPs (5 mg) were dispersed in 50 ml of sodium phosphate solution to prepare a MNP-salt mixture. 2 ml of SF/PEI mixtures (5 mg/ml) at different SF/PEI concentration ratios (as above) were then blended with 10 ml of MNP-salt mixtures and the resulting solutions were kept at room temperature (20 °C) for 6 h to allow the formation of MSPPs. The particles were then washed and collected with Neodymium magnets. Magnetic SF and magnetic PEI particles were prepared by the same method as controls.

2.5. Preparation of MSPP-ODN complexes

MSPP-ODN complexes were prepared by mixing the MSPP solutions with ODN solutions. An ODN aqueous solution of 0.2 mg/ml was prepared. MSPPs were dispersed in DI water to obtain MSPP solutions at different concentrations (0.2, 1.2, 2.4, 5, 10, 20 mg/ml). 100 μl of prepared ODN solution was then added to 100 μl MSPP solutions and mixed under gentle shaking until a homogenous dispersion was achieved. Finally, the mixed solution was incubated for 30 min at room temperature. The final ODN concentration in the mixed solution was fixed at 0.1 mg/ml and the MSPP concentrations were varied from 0.1 to 10 mg/ml to achieve different MSPP/ODN mass ratios (1:1, 6:1, 12:1, 25:1, 50:1, 100:1). MSPP/ODN mixed solutions with higher concentrations of ODN (1 or 2 mg/ml) and MSPPs (12 or 24 mg/ml) were also prepared with similar process. The prepared dispersions were diluted in PBS before added into cell cultures.

2.6. Particle characterization

2.6.1. Dynamic light scattering and zeta potential analysis

Particle aggregation size and zeta potential were carried out by a dynamic light scattering (DLS) analyser (NanoBrook 90 plus Pals Particle size Analyzer, Brookhaven Instrument, NY, USA). Particles were dispersed in DI water in a cuvette before placed in the sample cell. A diode laser with wavelength of 660 nm was used. All experiments were conducted at a measurement temperature of 18 °C controlled by a circulation bath. Three batches of samples were prepared and analysed.

2.6.2. Atomic force microscopy (AFM) analysis

The size and morphology of particles were characterised using Atomic Force Microscopy (AFM, Dimension Icon with ScanAsyst, Bruker Corporation, U.S.A.). Particle suspensions were dropped on mica substrates and air dried before placing on the sample stage. AFM measurements were conducted using SCANASYST-AIR tips and ScanAsyst mode. The data was analysed with NanoScope Analysis 1.5 software.

2.6.3. Transmission electron microscopy (TEM) analysis

SPPs or MSPPs were dispersed in DI water at the concentration of 0.1 mg/ml. The dispersions were then dropped onto TEM copper grids and incubated at room temperature for 30 s. Excess solution on grids was then removed with filter paper, by gently dapping the edge and allowing excess liquid to be absorbed prior to TEM imaging (Tecnai G2 Spirit, FEI, USA). An acceleration voltage of 80 kV was used and images were recorded using a Gatan Orius SC1000B bottom mounted digital camera and analysed in Gatan Digital Micrograph software (version 3.9.1).

2.7. Cytotoxicity and cell growth inhibition

MDA-MB-231 or HDF cells were seeded into 96-well plates with 200 μl of complete RPMI medium (supplemented with 10% foetal bovine serum (FBS) and 1% L-glutamine) at a density of 5×10^3 cells per well and incubated overnight at 37 °C under 5% CO_2 atmosphere. The medium was then removed, and the cells were washed twice with PBS buffer before being replaced with 180 μl serum-free medium. 20 μl of SPP-ODN or MSPP-ODN complex dispersions with different particle/ODN mass ratios were added into each well. SPP or MSPP solutions (20 μl) with equivalent amount of particles used for complexation with ODNs were added into wells. ODN solutions were also used as negative controls with dosages equivalent to the amount of ODNs used in complexes. Cells were incubated for 4 h initially being exposed to a magnetic field for 20 min. The serum-free medium was then removed and replaced with 200 μl complete medium and cells were cultured to a final duration of 3 days. Then 50 μl of MTT reagent (3 mg/ml) was added into each well and cells were cultured for another 3 h until the

purple precipitate was visible. The medium was then removed and 200 μl of DMSO was added into each well before placing plates on a shaker until purple precipitates in wells were fully dissolved. The absorbance of each well was measured at 570 nm with a plate reader (FLUOstar galaxy, BMG LABTECH, Germany).

2.8. Cell transfection and uptake

MDA-MB-231 and HDF cells were seeded in 6-well plates at a density of 5×10^5 cells per well with complete medium and incubated overnight at 37 °C and 5% CO_2. The cell culture mediums were removed, and cells were washed twice with PBS before incubation with serum-free medium. SPP-ODN or MSPP-ODN complexes were added into different wells and incubated for 5, 20 min or 1, 4, 24 h with and without initial exposure to a magnetic field for 5 or 20 min (the maximum exposure time is 20 min). ODNs were added as a negative control. Oligofectamine-ODN was used as a positive control with a standard incubation time for 4 h in serum-free medium. After incubation, cells were washed twice with PBS buffer before further incubation in the complete medium to a final duration of 24 h. The resulting cells were harvested with trypsin and analysed with The BD™ LSR II flow cytometer (BD Biosciences, USA) to investigate the ODN uptake. The data were analysed by the FlowJo v10 software.

2.9. Magnetically targeted delivery assay

MDA-MB-231 cells were seeded into 6-well plates (with 2 coverslips in each well) at a density of 3×10^5 cells per well with complete medium. After 24 h, cells were washed twice with PBS buffer before incubation in serum-free medium. Cells were incubated with naked ODNs, Oligofectamine-ODN, SPP-ODN and MSPP-ODN complexes for 4 h. The magnetically targeted delivery was conducted by placing a circular neodymium magnet under one of the coverslips in each well for 20 min at the start of incubation. After initial incubation, cells were washed twice with PBS buffer to remove free ODNs and transfection complexes followed by a further incubation in complete medium to a total incubation time of 24 h. The cells were then washed twice with PBS and fixed with 4% paraformaldehyde. The fixed cells were stained with Alexa Fluor 568 Phalloidin and DAPI for 1 h. The confocal fluorescence images of cellular uptake of ODNs were observed with an Inverted Zeiss LSM 510 NLO microscope (Zeiss, Germany) and analysed with LSM Image Browser software (version 4.2.0.121).

2.10. Statistical analysis

The statistical analysis of the data was carried out by using GraphPad Prism 7.02 (*t*-test).

3. Results and discussion

3.1. Characterization of SPPs and MSPPs

3.1.1. Size, zeta potential and morphology of SPPs

SF forms aggregates in high concentration salt solutions such as sodium phosphate. The salting-out of SF is resulted from the competition of free water molecules between the protein molecules and salt ions (Scopes, 2013). At low salt concentrations the hydrophobic amino acids in SF are protected by hydrophilic amino acids which interact with the surrounding water molecules (Scopes, 2013). With increasing salt concentration more water molecules are attracted by salt ions leading to a decrease in the number of water molecules interacting with SF proteins, therefore resulting in increased hydrophobic interactions between SF chains, inducing the formation of SF aggregates (Scopes, 2013). During salting-out, micellar-like structures are first formed due to the enhancement of hydrophobic interactions between SF protein chains, followed by further aggregation and finally particulate SF

globules (Lammel et al., 2010).

The addition of salt can also be used to induce the aggregation of PEI (Curtis et al., 2016). PEI is a cationic polymer with hydrophobic backbones and closely-spaced amines making PEI a highly positive charged polymer (Curtis et al., 2016). The intra-chain repulsion caused by the amine groups on the same chain keeps the polymer from aggregating (Curtis et al., 2016). If the charges on the hydrophobic chains are insufficient e.g. by increasing salt concentration (Curtis et al., 2016), the hydrophobic backbones will collapse and form aggregates (Dobrynin and Rubinstein, 1999; Chandler, 2005). Adding a small amount of salt into PEI solution increases the PEI solubility and prevents its aggregations due to the fact that the attractive interactions between hydrophobic chains are counterbalanced by the electrostatic repulsion at low ionic strength (Curtis et al., 2016). The solubility of PEI reached a maximum at 150 mM NaCl concentration. Further increasing the salt concentration resulted in the salt screening of the electrostatic repulsion therefore decreasing intra-chain repulsion resulting in PEI aggregations via hydrophobic interactions (Curtis et al., 2016).

PEI particles were prepared by adding PEI solution (5 mg/ml) into sodium phosphate solution (pH 8) at an ionic strength of 1.25 M. After an incubation time of 6 h at room temperature aggregations were observed. The particle size was then analysed using DLS as shown in Fig. 1a, which indicated that the mean diameter of PEI particles was 85 nm. The addition of different ratios of SF into the PEI solution resulted in the increasing of particle size (Fig. 1a). Increasing the SF ratio lead to accelerated aggregation of SPPs as well as increased particle yield. When using a mixture containing 90% SF (5 mg/ml) and 10% PEI (5 mg/ml), the SPP aggregation was almost immediate upon added into salt solution. As shown in Fig. 1a, the size of SPPs increased from 107 to 436 nm when increasing SF content from 10% to 90%.

This phenomenon is most likely due to the inter-chain attractions between positively charged PEI chains and negatively charged SF chains. When a small amount of SF was added to PEI solutions, negative SF chains were attracted and electrostatically bound to positive PEI chains, weakening the charge density of PEI chains. With increasing amount of SF, PEI chains are neutralized and the backbone charge becomes insufficient to keep the molecules extended after the mixtures being added into salt solutions (Curtis et al., 2016). This is supported by the SPPs zeta potential measurements (shown in Fig. 1a), where the zeta potential decreases with increasing SF content. A zeta potential of +50 mV was observed for PEI particles. The strong electrostatic repulsions among PEI particles resulted in small particles (85 nm). An addition of 10% SF in PEI solution reduced the zeta potential of SPPs to +45 mV, increasing the mean particle diameter to 107 nm (Fig. 1a). Further increasing the SF content lead to lower zeta potentials and larger SPP particle sizes, where 90% SF resulted in a zeta potential of +32 mV. At 95% SF content the SPPs were almost electroneutral (zeta

potential: +7.3 mV) and large amount of precipitate was observed. The changes of particle size and zeta potential dependant on the SF/PEI ratio give strong indication of hybrid particle formation.

In addition to DLS analysis the size and morphology of SPPs were also determined using AFM. As shown in Fig. 2a–f, spherical particles with smooth surfaces were observed. PEI-only particles (Fig. 2a) showed diameters ~80 nm, in contrast to SPPs, where particles with diameters of over 400 nm were observed for the highest SF content (90%, Fig. 2f), which is consistent with the particle sizes given by DLS. In order to reveal the structures of the SPPs, TEM analysis was undertaken. Fig. 2g shows small PEI particles with diameters of ~30 nm aggregated to form larger particles (~100 nm). The structures of SPPs with 50%, 75% and 90% of SF are shown in Fig. 2h, i&j, respectively. Increasing diameters of ~200 nm, ~260 nm and ~400 nm were observed from these particles respectively, which was consistent with the results given by DLS and AFM. SPPs with 90% of SF (SPP90) shown in Fig. 2j clearly show that the particle formed by the aggregation of many smaller particles with diameters ranging from 30 to 100 nm, confirming that increasing SF content resulted in lower surface charge and lead to particle aggregation.

3.1.2. Size, zeta potential and morphology of MPPs and MSPPs

MPPs were fabricated by adding PEI (5 mg/ml) to MNPs suspended in sodium phosphate solution. Zeta potential measurements revealed negative charges of −12.6 mV for MNPs and high positive charges of +48.5 mV for MPPs (see Fig. 1b), which are in agreement with previous reports by Wang et al. (2009) and Zhao et al. (2014). These measurements strongly suggest that negatively charged MNPs have been coated with positive PEI molecules which adsorb onto the surface of MNPs through electrostatic attractions and Van der Waals forces (McBain et al., 2007) before aggregating and entirely covering the MNP in the final salt solutions (Curtis et al., 2016). DLS measurements of MNPs revealed average particle diameters of 109 nm and increased to 131 nm after PEI coating (see Fig. 1b), similar to the results reported by Ota et al. (2013) previously.

The particles were further characterised by AFM to investigate the morphologies of MNPs, MPPs and MSPPs. AFM revealed that the MNPs exhibited rough surfaces with particle sizes ranging between 10 and 30 nm (Fig. 3a), while MPPs were ~110 nm in diameter (Fig. 3b) supporting the conclusion that the MNP surfaces were coated with PEI polymers. It should be noted that MNPs size measurements with AFM show a significantly smaller particle size than DLS measurements, which is most likely due to MNP particle aggregation occurring in the suspensions during the DLS measurement. Further to this, TEM analysis of MPPs reveals a core-shell type structure as shown in Fig. 3g. The core phase consisted of Fe_3O_4 nanoparticles, represented by the dark regions of the image compared to the shell structure of the PEI polymer in grey.
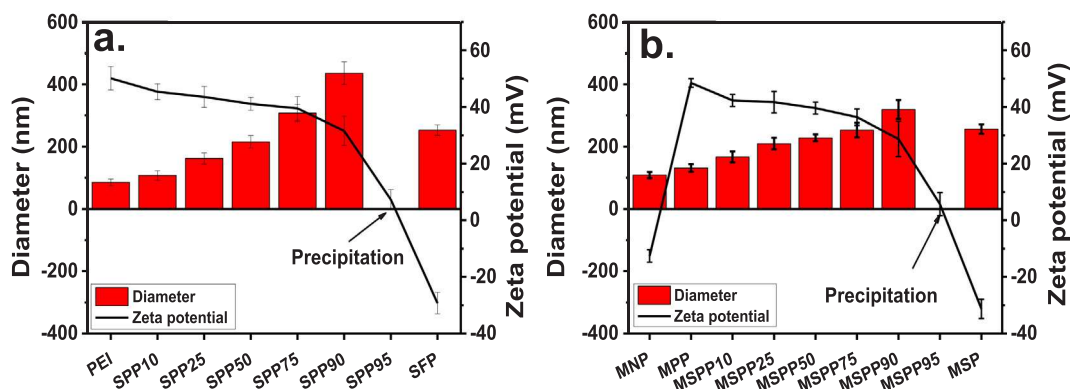
Fig. 1. Effect of SF (5 mg/ml)/PEI (5 mg/ml) ratio on the size and zeta potential of SPPs (a), and MSPPs (b). The increase of SF ratio resulted in the increase of the size of SPPs and MSPPs, and also resulted in the decrease of the zeta potential of SPPs and MSPPs. SPP (or MSPP) 10, 25, 50, 75, 90 & 95 represent SPPs (or MSPPs) with 10%, 25%, 50%, 75%, 90% & 95% of SF. The results are shown in mean ± SD, n ≥ 3.
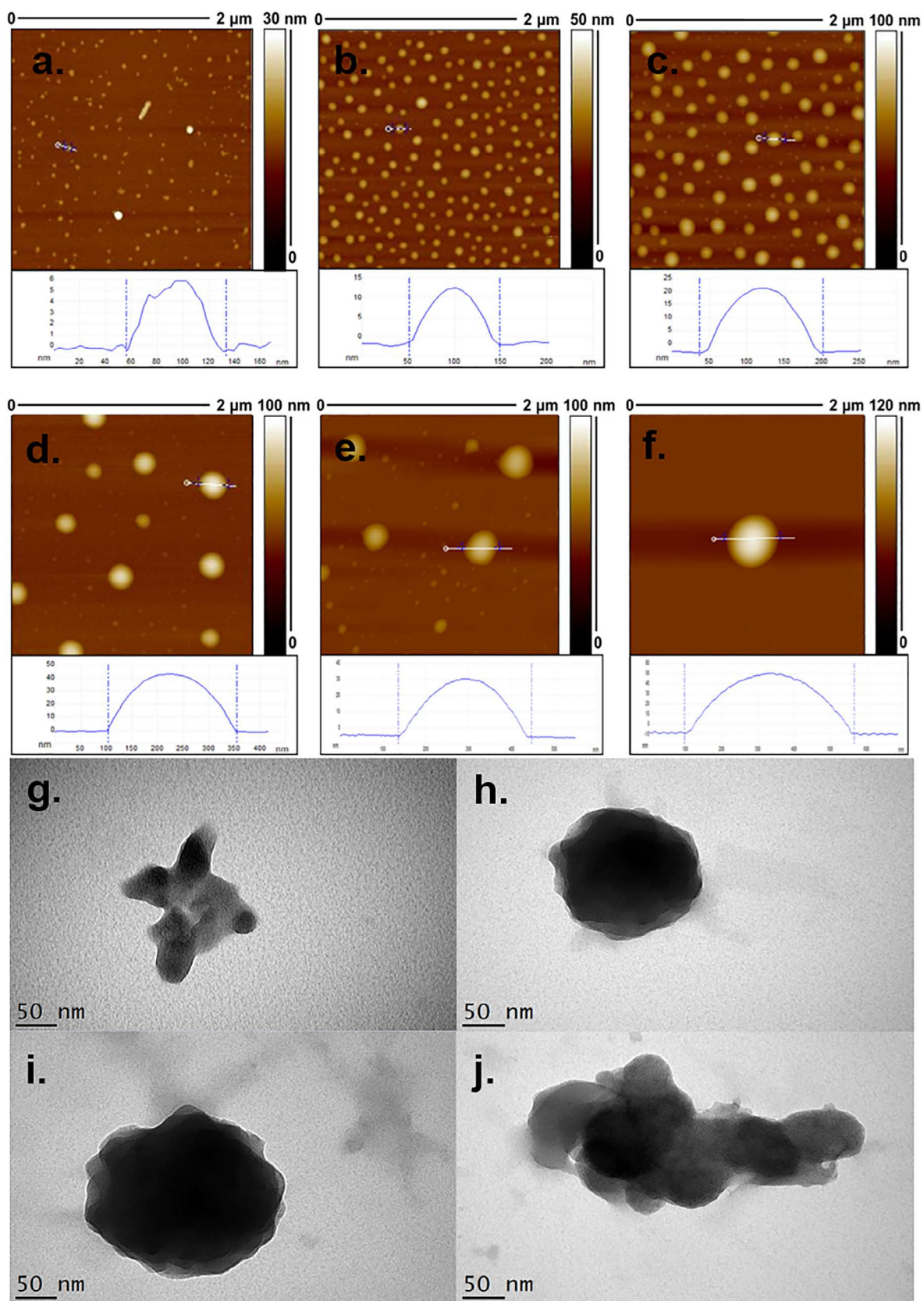
Fig. 2. AFM and TEM images of the PEI particles (a&g) and SPPs (b–j) with different amount of SF: 10% (b), 25% (c), 50% (d&h), 75% (e&i) and 90% (f&j). The increase of SF amount resulted in the increase of particle sizes.

Fig. 3. AFM and TEM images of the MNPs (a), MPPs (b&g), and MSPPs with 10% (c), 50% (d&h), 75% (e&i), and 90% (f&j) of SF.

TEM images clearly revealed (Fig. 3g) that smaller MPPs of the order of ~20 nm aggregated and formed larger aggregated particles of ~100 nm in diameter, consistent with the AFM data. Steitz et al. (2007) previously reported that coating with PEI polymers can bridge two or more particles together and form larger aggregations throu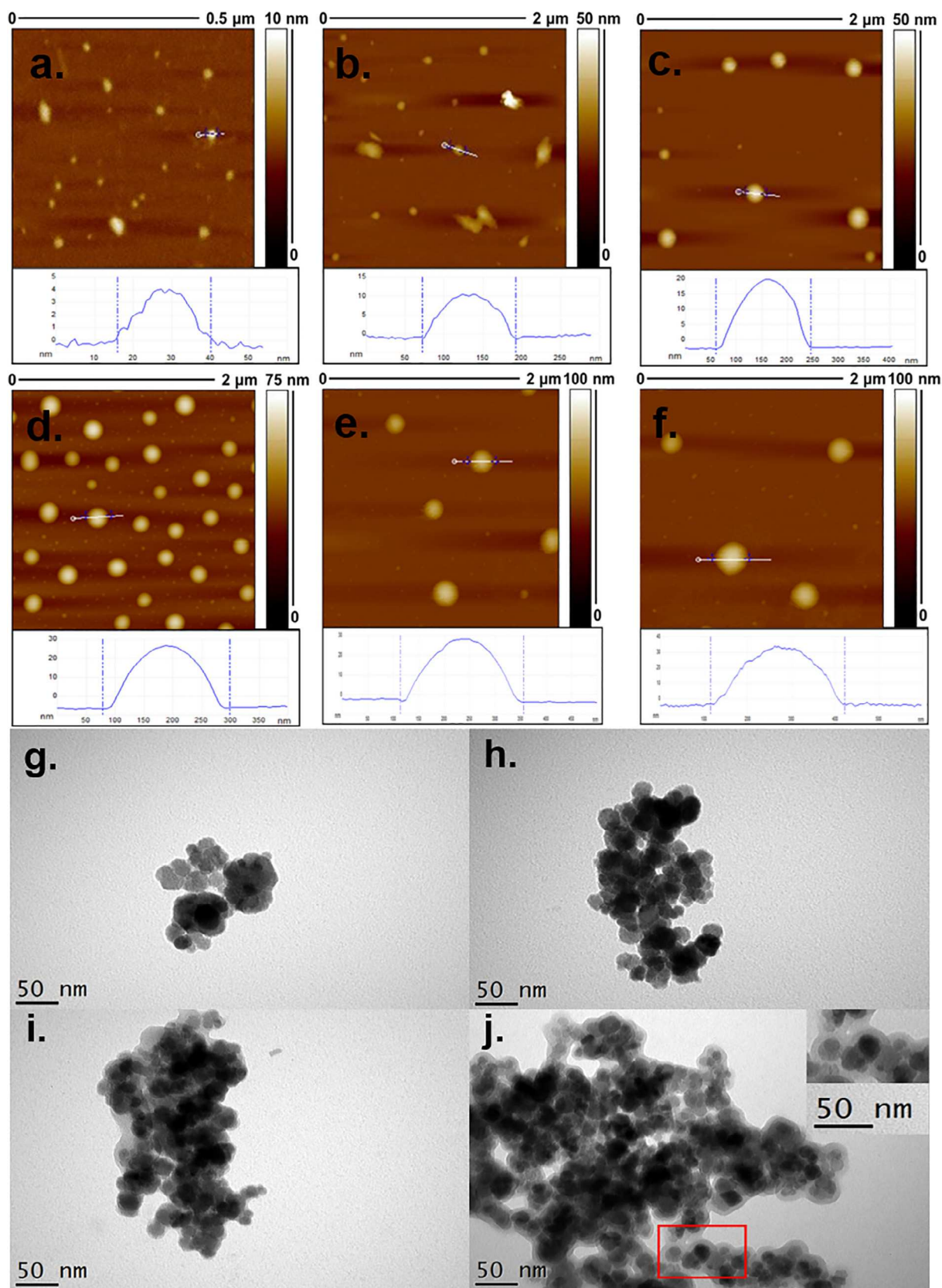gh Van der Waals forces. On the other hand, MPPs are strongly positively charged due to a large amount of amine groups in PEI, resulting in strong electrostatic repulsions among MPPs and thus enabling better dispersion of these particles. The balance between Van der Waals forces and electrostatic repulsions resulted in such aggregate size of MPPs. Changes of the electrostatic charges on the surface of the particles will however lead to different aggregate sizes.

Further to the synthesis of MPPs above, the PEI (5 mg/ml) was mixed with different ratios of SF (5 mg/ml) before they were coated onto MNPs. The resulting particle sizes and zeta potentials measured (by DLS) were also shown in Fig. 1b. The mixed polymer shell of SF and PEI resulted in different surface charges and aggregation sizes of MSPPs. The addition of SF reduced the zeta potential of MSPPs compared with MPPs indicating negatively charged SF and positively charged PEI had co-aggregated on the surface of MNPs. By altering the SF/PEI ratio both particle size and zeta potential are controllable as shown in Fig. 1b. For example, 10% of SF in PEI resulted in a decreased zeta potential of +42 mV and an increased average diameter of 167 nm for MSPPs. Increasing the SF to 90% resulted in even lower zeta potential (+29 mV) and larger particle diameter (319 nm). The increased aggregate size can be explained by reduced electrostatic repulsions between particles, causing MSPPs to form aggregates through Van der Waals forces more readily. At a SF content of 95% a near neutral sample was produced having a zeta potential of +5.7 mV with almost all the particles precipitated out, suggesting there was insufficient electrostatic repulsion between particles to keep them from aggregating.

Morphologies of MSPPs were analyzed by AFM and TEM. As shown in Fig. 3c–f, the size of MSPPs increased with increasing SF content, which is consistent with measurements by DLS. Spherical and smooth particles were observed, suggesting the surfaces of MNPs were coated by SF-PEI polymer mixture. Similar to SPPs, AFM images for MSPPs revealed smaller particles around larger ones (Fig. 3c–f), suggesting the large particles were aggregations of small MSPPs. TEM images of MSPPs (at 50%, 75% and 90%) shown in Fig. 3h–j reveal that MSPPs were formed by multiple Fe_3O_4 cores covered by SF-PEI shells. The inset in Fig. 3j is an enlarged section of the image (red boxed area). Altering the SF content did not show any effect on the size of the smaller core-shell magnetic nanoparticles which were consistently around 20 nm in diameter. However, the increased SF percentage resulted in larger aggregates supporting the previous AFM and DLS data.

Finally, it is worth to note that positive zeta potential in excess of +28 mV were observed even at low PEI contents (10%) in SF-PEI mixtures. This is due to the high charge density of PEI (Smits et al., 1993). This phenomenon is favorable for the fabrication of low toxic cationic carriers for DNA transfection. DNA is able to adsorb onto the carrier surface via electrostatic attractions, demonstrating the importance of positive charges for DNA adsorption (Zhang et al., 2016; Steitz et al., 2007).

3.2. Interaction of MSPPs with c-myc antisense ODNs

For successful gene transfection, vectors are normally required to condense the DNAs (Ono and Spain, 1999; Arscott et al., 1990; Andrushchenko et al., 2002). The mechanisms by which DNAs form complexes with transfection vectors has been reported and morphologies of the complexes have been previously characterized by AFM (Zhao et al., 2014; Andrushchenko et al., 2002; Danielsen et al., 2004; Volcke et al., 2006). Single stranded ODNs are different to plasmids and long linear DNAs in both molecular weight and topography which may result in different pathways in condensation and forming complexes (Chen et al., 2006). It is therefore important to investigate the formation of

MSPP-ODN complexes and their assembly mechanism. The morphologies of naked ODNs and the resulting complexes were characterized by AFM. For the naked ODN, spherical structures with diameters ranging from 30 to 40 nm and heights of 2 to 3 nm were observed (see Fig. 4a), similar to the ODN self-assembled structures previously reported by Costa et al. (2004). Nanowires were also observed, similar to the ones reported by Chiorcea-Paquim et al. (2013), having lengths of over 500 nm and heights ranging from 2.5 to 3.5 nm (Fig. 4a). As the ODNs used in this research are only 15 nucleotides, the large scaled nanostructure is most likely to be a higher order structure of self-assembled ODNs (Chen et al., 2006; Costa et al., 2004; Chiorcea-Paquim et al., 2013; Chiorcea-Paquim et al., 2013). The self-assembly of guanine (G) rich ODNs into higher order nanostructures such as networks and long nanowires (Chiorcea-Paquim et al., 2013) has been previously reported (Chen et al., 2006; Costa et al., 2004; Chiorcea-Paquim et al., 2013; Chiorcea-Paquim et al., 2013).
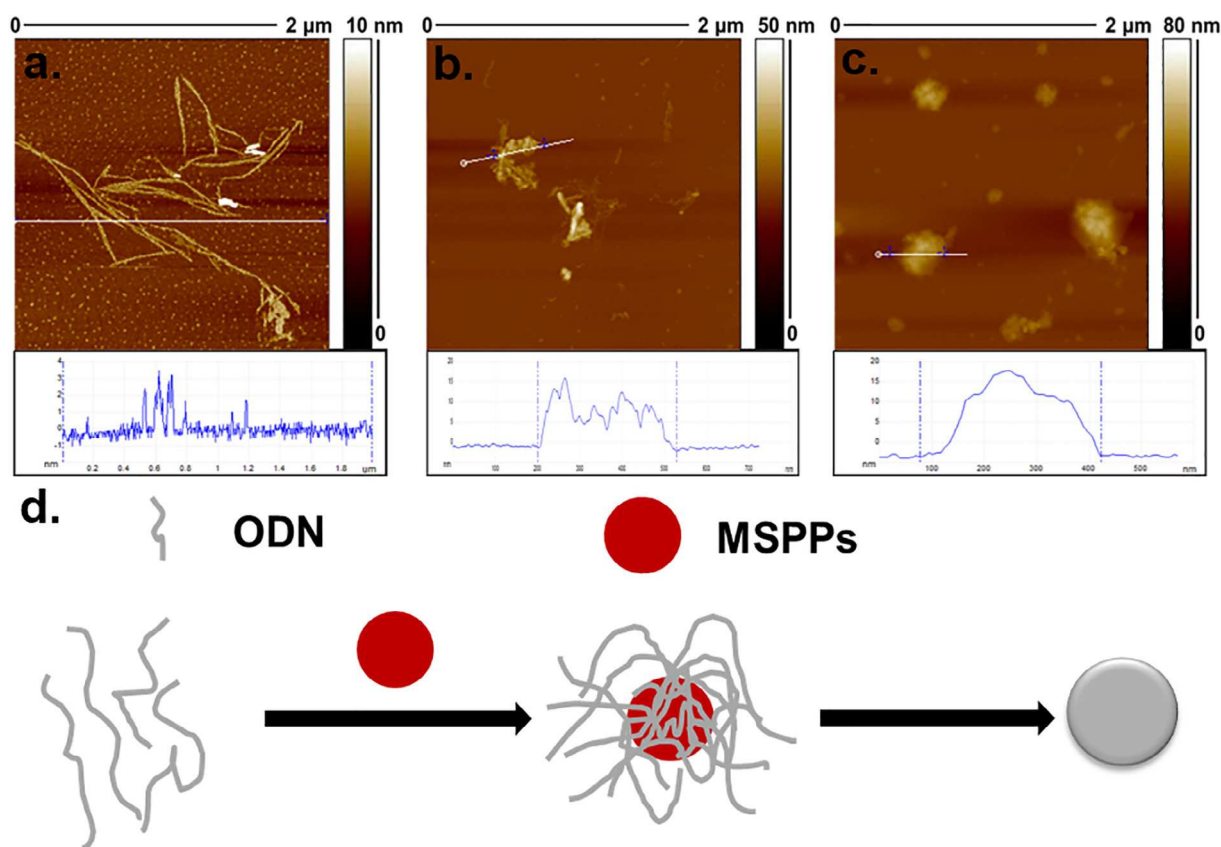
Fig. 4b&c are representative AFM images of ODNs that were mixed under gentle shaking with MSPPs with 90% SF (MSPP90) at a mass ratio of 12:1 after 30 s (b) and 30 min (c) condensation time. After 30 s, condensed nanofiber-like structures and aggregations of nanowires were observed (Fig. 4b), similar to the nanostructures reported by Chen et al. (2006) who mixed a 21-nt ODN with polypropyleneimine (PPI) followed by a 10 min condensation time. The height of the condensed nanofibers ranged from 2 to 15 nm and diameters of aggregated structures from 80 to 300 nm, suggesting that the free ODNs were condensed by MSPP90. After 30 min condensation time well-condensed MSPP-ODN complexes were formed as shown in Fig. 4c, consisting of spheroidal particles with diameters of 100 nm–350 nm and heights ranging from 10 to 20 nm. Rough surfaces morphologies were observed as a result of ODN complexation on particle surfaces. Comparable spheroidal condensates have also been reported in previous studies (Andrushchenko et al., 2002; Danielsen et al., 2004; Volcke et al., 2006; Chen et al., 2006; Costa et al., 2004). ODNs were most likely interacted with MSPPs through electrostatic attractions and produce nanofibers during the initial condensation process (Fig. 4d). At longer condensation times (30 min), ODN chains tightly wrapped around the MSPPs and spheroidal MSPP-ODN complexes were formed.

3.3. In vitro cytotoxicity assay

3.3.1. Inhibition effect of MSPPs and MSPP-ODN on MDA-MB-231 cells

C-myc oncogene is an evolutionarily conserved gene expressed in many cell types including MDA-MB-231 breast cancer cells (Junghans et al., 2000). It is often associated with many essential biological processes including cell growth, proliferation, transformation and apoptosis (Junghans et al., 2000; Gu et al., 2017). Disordered expression of the c-myc gene will lead to malignant transformation of cells (Junghans et al., 2000). Down regulation of the expression of c-myc by exposing the cancer cells to c-myc antisense ODN has been reported to be able to inhibit cancer cell growth (Junghans et al., 2000; Leonetti et al., 1996; Watson et al., 1991). c-myc antisense ODN is a single-stranded nucleic acid designed to specifically bind to the target mRNA through the Watson-Crick base pair complementarity to form duplexes (Santhakumaran et al., 2004). This therefore blocks the translation of the target gene or alternatively, the RNase H can be activated to digest the specific mRNA (Zhao et al., 2007; Santhakumaran et al., 2004). High efficacy was expected for antisense ODNs due to its specificity to target mRNAs (Santhakumaran et al., 2004). However, the application of c-myc antisense ODNs is limited by major hurdles such as poor delivery and cellular uptake of naked ODNs into the target tissue along with their poor *in vivo* stability (Zhao et al., 2007; Santhakumaran et al., 2004; Mumcuoglu et al., 2016; Petrilli et al., 2014). The inherent hydrophilicity and negative charges of ODNs make it very difficult for them to approach and cross the hydrophobic cell membranes into the cytoplasm or nucleus (Gangar et al., 2013). Therefore, large amount of ODNs and long incubation times are needed for the observation of any

Fig. 4. AFM images of ODNs (a) and MSPP90-ODN complexes (b&c). The AFM images were taken after 30 s (b) and 30 min (c) condensation respectively. MSPP90/ODN mass ratio was fixed at 12:1. (d) Schematic representation of the possible mechanism for the condensation of ODNs by MSPPs. ODN chains wrapped around the MSPPs to form spheroidal MSPP-ODN complexes.

cell growth inhibition effect when the cells are treated with naked ODN (Balaji et al., 1997; Leonetti et al., 1996; Watson et al., 1991). For example, in the study by Watson et al. (1991) 4 days were required for the observation of initial inhibition for MDA-MB-231 cells exposed to 5 μM c-myc antisense ODN. In another study, Leonetti et al. (1996) added 100 μg/ml c-myc antisense ODN to M14 cells and only after 4 days growth inhibition could be observed. These illustrate the need for efficient transfection systems for antisense gene delivery to solve the above problems (Pan et al., 2007). Various vectors have previously been developed and have shown improved inhibition efficiency at lower ODN dosages (Zhao et al., 2007; Pan et al., 2007; Sarkar et al., 2005; Pan et al., 2009). However it is clear that vast improvement is still needed for efficient systems.

MTT assay in Fig. 5 shows that negligible growth inhibition was observed for MDA-MB-231 cells treated with naked ODNs (red columns), indicating that efficient transfection was difficult for naked ODNs due to its poor cellular uptake. The increased dosage of MPPs and MSPPs resulted in decreased viability of MDA-MB-231 cells treated with those particles, indicating that MPPs and MSPPs possessed dose-dependent cytotoxicity to MDA-MB-231 cells. The introduction of SF into the MPPs system reduced the cytotoxicity of MPPs. Cells treated with MSPPs (at 50–90% SF) showed a higher viability than those treated with MPPs (blue columns). At the same MSPP dose, cell viability increased with the increase of SF content in MSPPs. For example, at the concentration of 50 μg/ml (associated with the MSPP/ODN ratio of 50:1) MDA-MB-231 cells showed the viabilities of 58%, 73%, 77% and 85% after treated with MPPs, and MSPPs with 50%, 75% and 90% of SF respectively, giving strong evidence that the addition of SF resulted in reduced cytotoxicity of MSPPs.

By increasing mass ratios of MPPs/ODN from 1:1 to 100:1 a clear decrease in cell viability can be seen (Fig. 5a), where at lower mass

ratios from 1:1 to 25:1 cells treated with MPP-ODN exhibited a significantly lower viability to those treated with MPPs. All these lowered cell viabilities indicate that c-myc antisense ODN induced cell growth inhibition occurred. However, at higher ratios (50:1–100:1) no significant difference on viabilities were observed between cells treated with MPPs and MPP-ODN, suggests the inhibited cell growth mainly have been a result from the cytotoxicity of MPPs and shield the effect of ODNs. On the other hand, as shown in Fig. 5b–d, on average a ~20% lower viability for MDA-MB-231 cells treated with MSPPs (50–90% SF)-ODN to those treated with MSPPs (50–90% SF) was observed at the whole ratio range investigated, indicating that MSPPs with SF are capable of transfecting the ODN for the inhibition of cell growth. It is important to note that even at higher particle/ODN ratios (50:1–100:1) cells showed significantly lower viabilities after treated with MSPP-ODN to those treated with MSPPs (50–90% SF), suggesting the reduced viabilities were mainly attributed to the function of ODN instead of toxicity of MSPPs. These results indicated that with reduced cytotoxicity compared to MPPs, MSPPs (50–90% SF) allow the efficient growth inhibition performance of ODN without bringing significant cytotoxicity of carriers to cells, which is desired in gene transfection.

Since MSPP90 showed the lowest toxicity among these particles (MSPPs 50–90% SF) and is still capable of transfecting the c-myc antisense ODN to cause the growth inhibition of MDA-MB-231 cells, it is of interest to investigate its optimum mass ratio with ODN to achieve high inhibition effect from ODN while avoid additional cytotoxicity from MSPP90. As shown in Fig. 5d, when the MSPP/ODN mass ratio was 1:1, MSPP90-ODN exhibited the lower inhibition effect than other MSPP-ODN complexes, which was most likely because insufficient MSPP90 were provided at such mass ratio. Increased mass ratio from 1:1 to 12:1 resulted in decreased viabilities for cells treated with MSPP90-ODN, suggesting the growth inhibition effect was enhanced
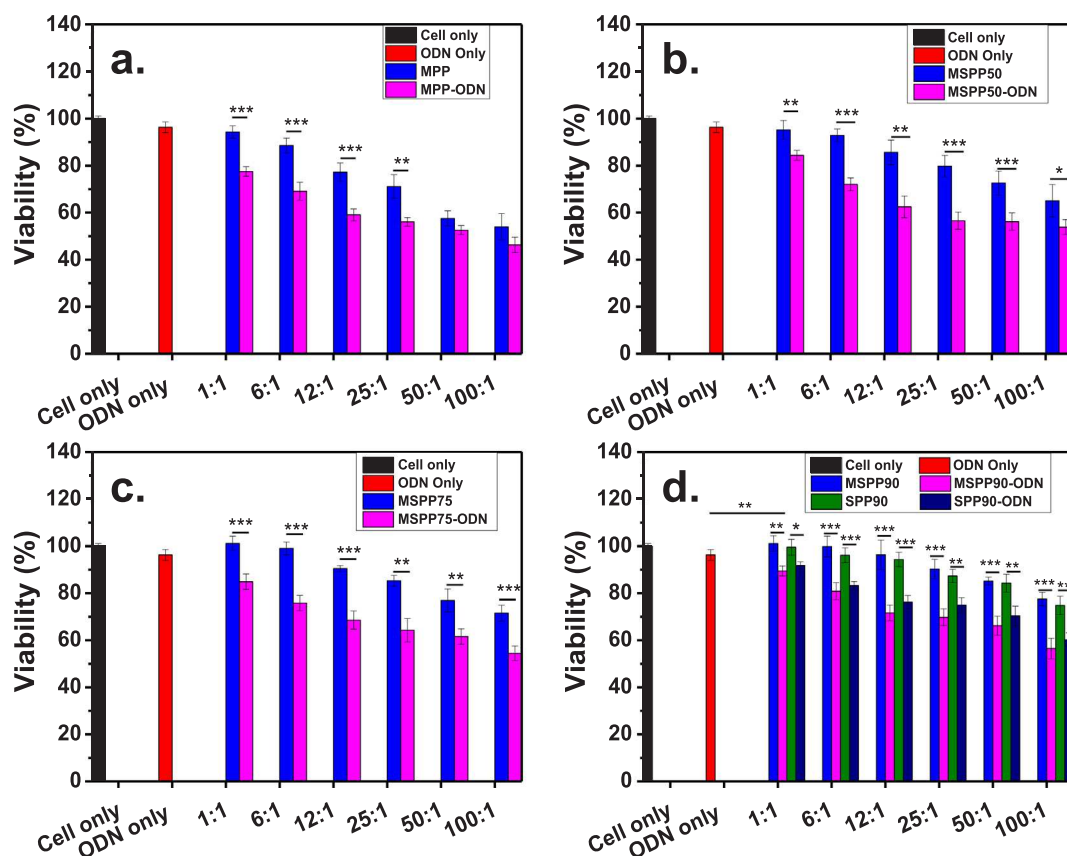
Fig. 5. MTT assay of MDA-MB-231 cells after 72 h incubation with different complexes: MPP-ODN (a), MSPP50-ODN (b), MSPP75-ODN (c), SPP90 and MSPP90-ODN (d) at different particle/ODN mass ratios (1:1–100:1). Complexes were added into serum-free MDA-MB-231 cell cultures for a 4 h transfection time, after which cells were washed with PBS and further incubated in complete mediums to a final duration of 3 days. At the beginning of transfection, the cells were exposed to a magnetic field for 20 min. Corresponding carriers and ODN-only with the amounts equivalent to the dosages in complexes were also used as controls to investigate their toxicity to MDA-MD-231 cells. The dosages of ODN were fixed at 1 μg/ml. The results are shown in mean ± SD, n = 4. The statistical significance is expressed as *** p < 0.001, ** p < 0.01, * p < 0.05.

with increased amount of MSPPs in MSPP90-ODN, which is most likely because the increased surface charge of complexes making them easier to interact with cell membrane and to be internalized. With further increase of the MSPP90/ODN ratio from 12:1 to 25:1 the viability of MSPP90 treated cells decreased from 96% to 90% without observation of significant viability decrease for cells treated with MSPP90-ODN complexes (only from 72% to 70%), indicated that the optimum MSPP90-ODN mass ratio for MDA-MB-231 cell growth inhibition at the ODN concentration of 1 μg/ml was 12:1. MDA-MB-231 cells treated with SPP90 and SPP90-ODN showed a similar growth inhibition pattern to those treated with MSPP90 and MSPP90-ODN, suggesting both particles possess similar cytotoxicity towards MDA-MB-231 cells.

It has been previously reported that the significant cytotoxicity of PEI is thought to be mainly due to its high amine content that resulted in high cationic charge density (Seow et al., 2013; Xue et al., 2014; Bansal et al., 2016; Ghiamkazemi et al., 2010). Free PEI molecules can interact with negatively charged substances such as serum proteins or even red blood cells to form aggregates which can adhere to tissue surfaces to cause significant cell damage (Xue et al., 2014). PEI is also able to interact with proteins inside the cell and therefore interfere with critical intracellular processes (Forrest et al., 2003). Many studies have been conducted to reduce the surface charge of PEI based transfection systems in order to minimum their cytotoxicity. For example, Xue et al. (2013) encapsulated hexadecylated-PEI polymers/siRNA complexes in negative charged lipids, the resulting surface charge of encapsulated complexes were decreased as well as the cytotoxicity compared with un-encapsulated PEI complexes. In another example, Liu et al. (2014) designed ASF/PEI/DNA ternary complexes by coating negatively

charged *Antheraea pernyi* silk fibroin (ASF) onto the surface of PEI/DNA complexes. The coating of ASF resulted in fewer surface charges and therefore a higher viability of cells transfected with ASF/PEI/DNA ternary complexes was observed compared to those transfected by PEI/DNA complexes. Therefore, it is believed that the reduced cytotoxicity of MSPPs is resulted from the reduced surface charge on these particles.

3.3.2. Concentration effect of particles/complexes on MDA-MB-231 and HDF cells

To investigate the inhibition effect of MSPP-ODN and SPP-ODN at different concentrations on cancer and normal cells, MDA-MB-231 breast cancer cells and human dermal fibroblast (HDF) were selected and treated with SPP90-ODN, MSPP90-ODN, SPP90 and MSPP90. MSPP90 was chosen because it exhibited the lowest cytotoxicity among MSPPs with different SF percentages and SPP90 was chosen as a comparison with MSPP90. MSPP90 and SPP90 were mixed with ODN at a mass ratio of 12:1 before incubating with MDA-MB-231 or HDF cells in serum-free medium for 4 h. The final concentrations of ODN in medium were 1, 5 and 10 μg/ml. A magnet plate was placed below the cells for the first 20 min of the initial incubation. After initial incubation, the cells were washed twice with PBS to remove any un-internalized particles and complexes before incubation in complete medium for a final duration of 3 days.

As shown in Fig. 6, naked ODN showed negligible growth inhibition effect on both MDA-MB-231 cells and HDF cells at the concentrations studied, suggesting that the growth inhibition effect of naked ODN was poor to both cells due to its poor internalization properties (Zhao et al., 2007; Santhakumaran et al., 2004; Mumcuoglu et al., 2016; Petrilli
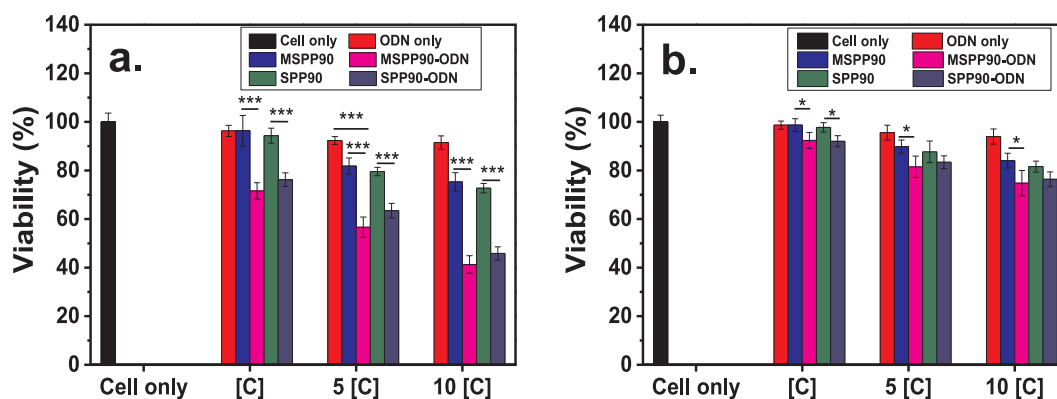
Fig. 6. Concentration effect of particles and complexes on breast cancer cells (a) and HDF cells (b). MDA-MB-231 cells and HDF cells were incubated with ODNs, MSPP90, SPP90, MSPP90-ODN, SPP90-ODN complexes for 4 h in serum-free medium. At the beginning, the cells were treated with an external magnetic field for 20 min. After the initial transfection, cells were washed twice with PBS buffer and incubated in complete medium for a final duration of 3 days. [C] = 12 μg/ml MSPP90 or SPP90 + 1 μg/ml ODN. Equivalent amount of ODN, MSPP90 and SPP90 were used as controls. The results are shown in mean ± SD, n = 4. The statistical significance is expressed as ***p < 0.001, **p < 0.01, *p < 0.05.

et al., 2014). Increasing the concentration of MSPP90 in medium resulted in decreased viability of MDA-MB-231 cells, which is consistent with the previous results obtained (see Fig. 5). This result strongly suggests that MSPP90 possess dose-dependent cytotoxicity to MDA-MB-231 cancer cells. After treatment with MSPP90-ODN, MDA-MB-231 cells showed significantly lower viability than cells treated with naked ODN and MSPP90, suggesting the complexation with MSPP90 have improved the effect of ODN. With the increased concentration from 1 [C] to 5 [C] and 10 [C], the viability of MDA-MB-231 cells treated with MSPP90-ODN decreased from 72% to 57% and 41%. While cells treated with MSPP90 showed the decreased viability of 96%, 82% and 75%. This result suggested that enhanced growth inhibition effect of MSPP90-ODN can be achieved without brought massive cytotoxicity from MSPP90.

Fig. 6b presents the viability of HDF cells after being treated with naked ODNs, MSPP90, SPP90 and their ODN complexes. It was observed that HDF cells were less affected by the particles and complexes. For example, after both cell lines being treated with MSPP90-ODN at the same concentration (1[C]), HDF cells exhibited a higher viability (92%) compared to that of MDA-MB-231 cells (72%). This is because cancer cells tend to exhibit a higher uptake efficiency on particles than normal cells due to the higher metabolic activity of cancer cells (Chaves et al., 2017) which leads to the overexpression of receptors on their surface and increases the available binding sites (Chaves et al., 2017; Kettler et al., 2014; Kohler et al., 2005). Furthermore, it has been reported that differences in cell-cell interactions between normal cells and cancer cells can also lead to faster particle uptake for cancer cells than normal cells (Gal et al., 2015). Gal et al. (2015) compared the internalization of polystyrene particle by MDA-MB-231 breast cancer cells and MCF-10A benign cells. The result indicates that cancer cells uniformly internalize particles in larger amounts and higher rate. However, only cells at the edge of a growing colony of benign cells are able to internalize particles (Gal et al., 2015). This is due to the fact that normal, adherent cells maintain tight cell-cell connections (Hazan et al., 2000). In contrast, cell-cell and cell-matrix interactions are less important for cancer cells, and particles can thus be internalized into any cell on the plate at high rates (Gal et al., 2015; Hazan et al., 2000). Therefore, it can be assumed that MDA-MB-231 cancer cells have taken up more MSPP90-ODN compared to HDF cells, which in turn resulted in the lower viability of MDA-MB-231 cells.
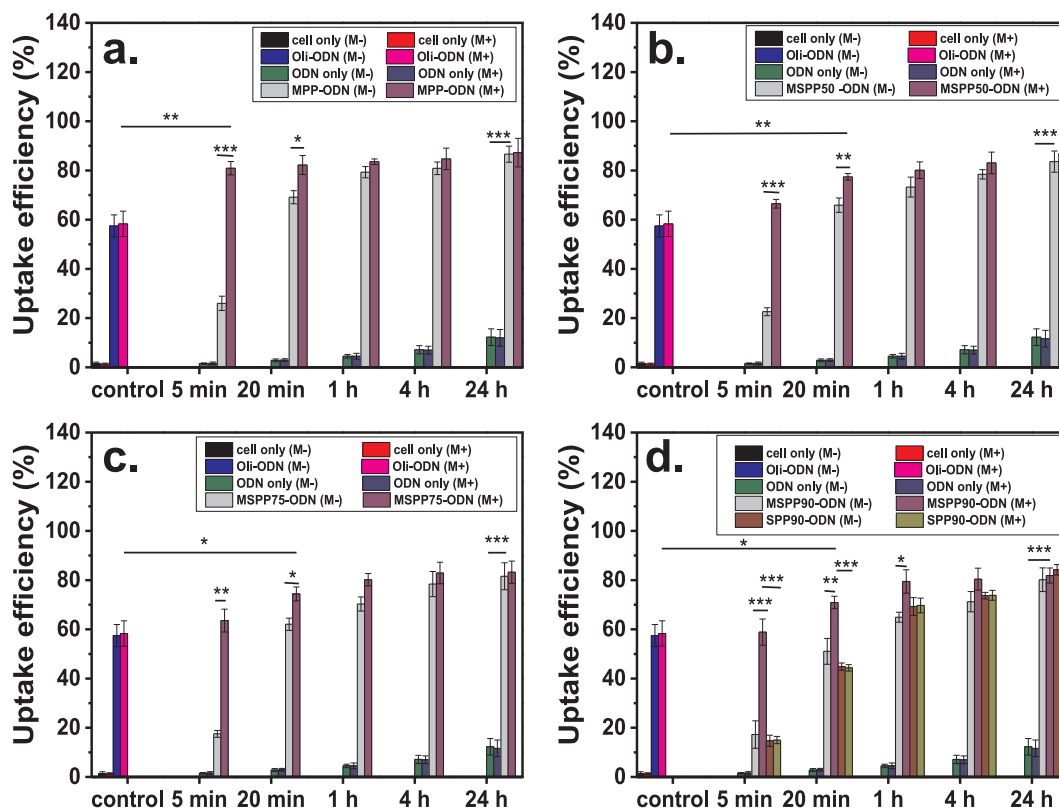
3.4. Cellular uptake assays

### 3.4.1. Uptake efficiency of MSPP-ODN and SPP90-ODN on MDA-MB-231 cells

Slow vector accumulation and the consequently low vector concentration at target tissues is reported as a strong obstacle for efficient gene transfection (Luo and Saltzman, 2000). By applying a magnetic field, magnetic vectors combining DNAs can be rapidly concentrated onto the surface of target cells which can facilitate complex internalization and enhanced transfection efficiency (Ma et al., 2011). This is also known as 'magnetofection'. For non-magnetofection vectors, their improved accumulation property is based on their designed biophysical properties or coupling with targeting ligands. However, in practise, it has been proved insufficient for rapid accumulation on target sites (Ma et al., 2011). On the other hand, magnetofection has shown outstanding performance in rapid transfection (Ma et al., 2011; Mykhaylyk et al., 2007; Krötz et al., 2003). Mykhaylyk et al. (2007) compared the transfection performance of magnetic and non-magnetic complexes exposed to a magnetic field. Their data showed that the magnetic complexes concentrated onto the surface of target cells and consequently transfection efficiencies were found 1000-fold higher than the transfections conducted with non-magnetic vectors (Mykhaylyk et al., 2007). Krötz et al. (2003) reported that magnetic particle-ODN complexes can be transfected into 84% of human umbilical vein endothelial cells within 15 min followed by nuclear accumulation within 2 h when exposed to a magnetic field, this is substantially faster than non-magnetofection methods which generally require 24 h incubation times.

To investigate the uptake kinetics of MPPs, MSPPs and SPPs, particles were complexed with fluorescence labelled ODNs at the mass ratio of 12:1. The final concentration of ODN was fixed at 1 μg/ml. The transfection experiment was conducted as described in Section 2.8. As shown in Fig. 7a, with magnetofection, 81% of MDA-MB-231 cells incubated with MPP-ODN took up the complexes with 5 min of incubation which was followed by washing the cells in PBS buffer twice and 24 h of further cultivation in complete medium. This resulted in a 3.1 fold increase of transfected cells compared with cells treated with MPP-ODN without a magnetic field (26%). This result supports previous studies which claimed that magnetofection can provide outstanding performance in rapid transfection compared to non-magnetofection (Ma et al., 2011; Mykhaylyk et al., 2007; Krötz et al., 2003). Increasing magnetofection time to 20 min only resulted in an increased uptake efficiency of 1% (from 81% to 82%). A further increase to the magnetofection to 24 h finally resulted in the highest uptake efficiency of 88%. This indicated that most MPP-ODN complexes were concentrated

Fig. 7. Cellular uptake assays of MPP-ODN (a), MSPP50-ODN (b), MSPP75-ODN (c), MSPP90-ODN and SPP90-ODN (d) complexes for MDA-MB-231 cells. The cell only and ODNs only are used as negative controls with the dosages of ODNs equivalent to the amount of ODNs used for the complexes. Oligofectamine-ODN was used as a positive control with a standard transfection time of 4 h. The concentration of the complexes was fixed at 12 µg/ml MSPPs + 1 µg/ml ODN. Cells were incubated with ODN or transfection complexes for 5 min – 24 h with (M +) or without (M −) the presence of an external magnetic field for a maximum of 20 min. The cells were then washed twice with PBS buffer and cultured with complete medium until to a final duration of 24 h before the FACS analysis. The results are shown in mean ± SD, n ≥ 3. The statistical significance is expressed as $^{***}p < 0.001$, $^{**}p < 0.01$, $^{*}p < 0.05$.
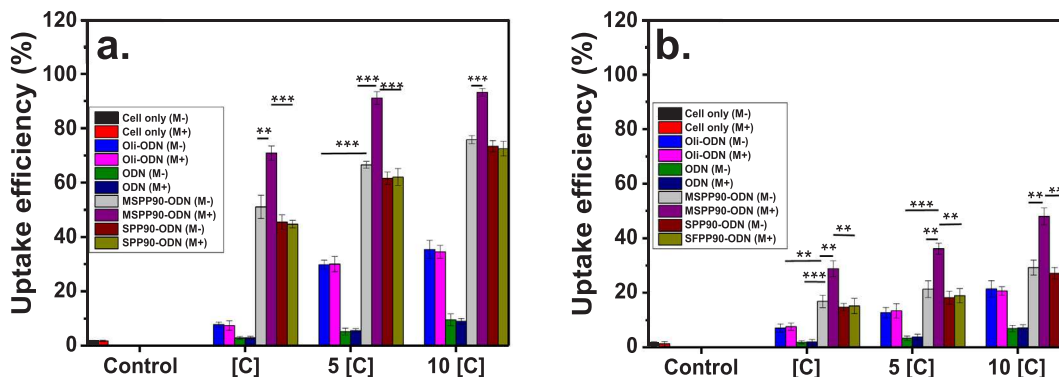

Fig. 8. Cellular uptake assays of MDA-MB-231 cells (a) and HDF cells (b) after treated with MSPP90-ODN and SPP90-ODN at different concentrations. The cell-only and ODNs-only are used as negative controls with the ODN dosages equivalent to the amount used for the complexes. Oligofectamine-ODN was used as a positive control. Cells were incubated with ODN or complexes for 20 min with (M +) or without (M −) the presence of an external magnetic field. After the initial transfection, cells were washed twice with PBS and incubated in complete medium to a final duration of 24 h before the FACS analysis. The MSPP90/ODN and SPP90/ODN mass ratio was fixed at 12:1. [C] = 12 µg/ml MSPP90 or SPP90 + 1 µg/ml ODN. The results are shown in mean ± SD, n = 3. The statistical significance is expressed as $^{***}p < 0.001$, $^{**}p < 0.01$, $^{*}p < 0.05$.

on the surface of cells within the first 5 min and extending the magnetofection time did not significantly increase the uptake efficiency. The result is in agreement with Krötz et al. (2003) who found no further enhancement of uptake efficiency was observed when extending the magnetofection time from 15 min to 24 h for human umbilical vein endothelial cells incubated with p22phox-antisens ODN containing magnetic vectors. For the MMDA-MB-231 cells treated with MPP-ODN without the presence of a magnetic field, increasing transfection time to 20 min increased the uptake efficiency by 43% (from 26% to 69%) and

a further increase to a total of 86% was seen for a transection time of 24 h, showing a clear time-dependent uptake of complexes through non-magnetofection. This is because the association of vectors to cells is a diffusion-limited process (Plank et al., 2003) which means only a fraction of the vectors interacted with the cells within the initial short period (e.g. 5 min). Therefore, increasing transfection time resulted in the significantly increase of complex uptake (Plank et al., 2003).

After 4 h transfection with Oligofectamine-ODN, ODNs uptake was found 58.3% for cells exposed to the magnetic field and 57.5% for cells
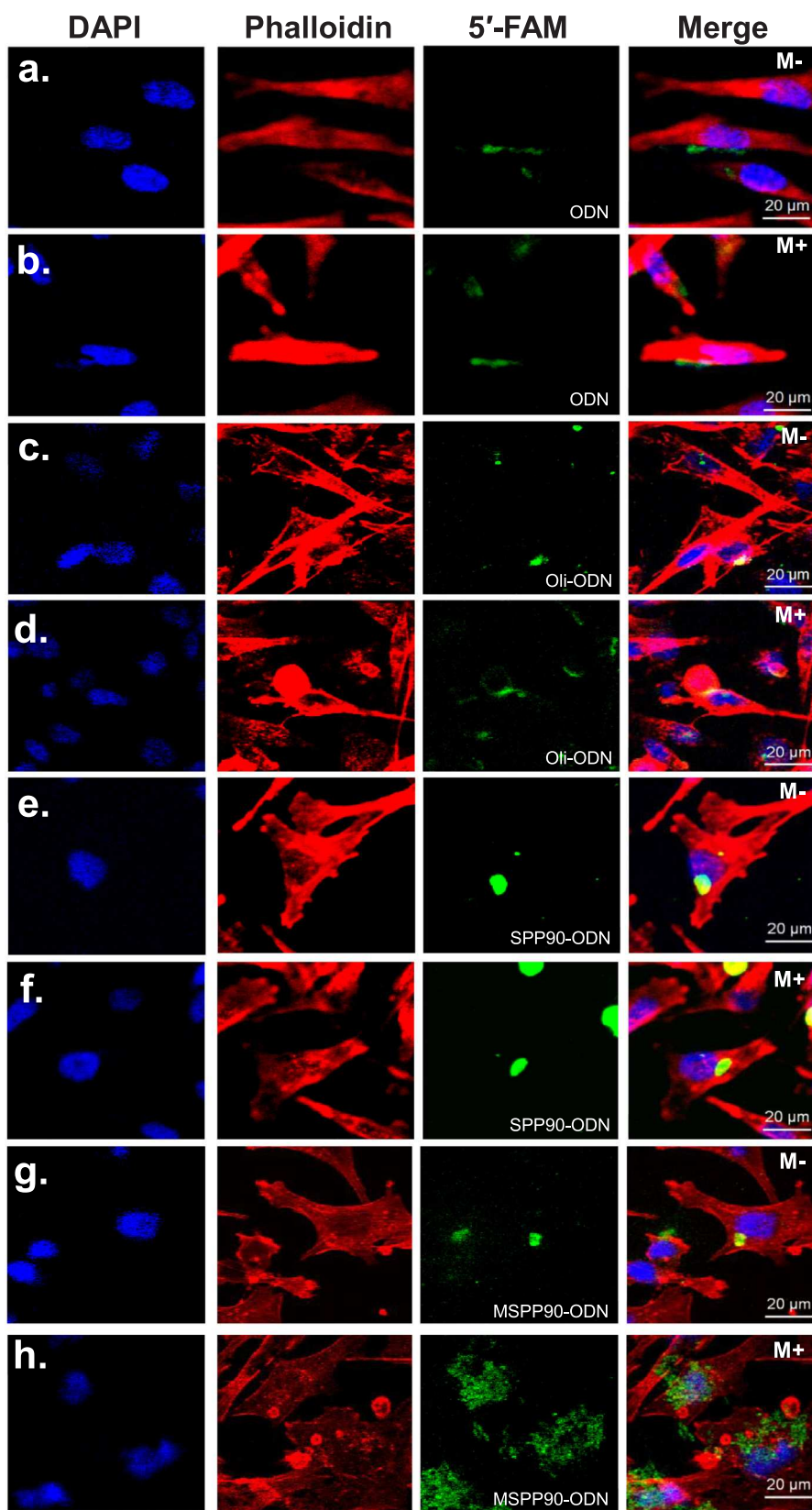
Fig. 9. Confocal microscopic images of MDA-MB-231 cells incubated with naked ODNs (a&b), Oligofectamine-ODN (c&d), SPP90-ODN (e&f) and MSPP90-ODN (g& h). ODNs were labelled with 5′-FAM (green). Cell nucleus and cytoskeleton were stained with DAPI (blue) and Alexa Fluor 568 Phalloidin (red). M+ indicates the presence of a magnet during the incubation and M− indicates the absence of the magnet. (For interpretation of the references to colour in this figure legend, the reader is referred to the web version of this article.)

not exposed to a magnetic field. This clearly suggests that Oligofectamine-ODN transfection is not dependant on the presence of a magnetic field. The uptake efficiency of Oligofectamine-ODN transfection for 4 h is lower than that of MPP-ODN for 4 h without the presence of magnetic field, which is most likely due to the faster sedimentation of MPP-ODN than Oligofectamine-ODN due to the higher density of MPPs. No significant differences were observed for cells incubated with naked ODNs with or without the presence of a magnetic field. Only 1.5% (M−) and 1.6% (M+) of total cells took up ODNs after being incubated with naked ODNs for 5 min. The uptake efficiency appeared to be time dependent. However, only 12.3% (M−) and 11.6% (M+) uptake efficiencies were achieved when cells were incubated with naked ODNs for 24 h, indicating that it is difficult for naked ODNs to be taken up by MDA-MB-231 cells. This explains the negligible reduction of cell viability by naked ODNs.

The uptake kinetics of MSPP-ODN complexes are represented in Fig. 7b–d. With the short magnetofection time of 5 min, 67%, 64% and 59% uptake efficiencies were achieved by MDA-MB-231 cells treated with MSPP50, MSPP75 and MSPP90, respectively. In contrast, only 23%, 18% and 17% of ODN uptake efficiencies were achieved for cells treated with MSPP50, MSPP75 and MSPP90 through non-magnetofection. This clearly shows that the uptake efficiency of ODNs can be drastically improved by MSPPs trough magnetofection.

On the other hand, Fig. 7b–d revealed that the uptake efficiencies of MSPP-ODN were time dependent. With increased magnetofection time from 5 min to 20 min, significant increased uptake efficiencies (over 70%) were observed for MDA-MB-231 cells treated with MSPP-ODN with magnetic field, suggesting longer transfection period helped the accumulation of MSPP-ODN to the cell surface. The difference in uptake over time is presumably due to the difference in positive surface charges between MPPs and MSPPs. As mentioned in Section 3.1.2, the positive charges of MSPPs are lower than those of MPPs due to the introduction of negatively charged SF and with the increase of SF the surface charges of MSPPs decrease further. The decreased surface charges of MSPPs may be the reason why longer magnetofection times are required for MSPP-ODN to achieve uptake efficiencies similar to MPP-ODN. However, it is worth to note that a considerably high uptake efficiency (over 70% compare to ~80% final uptake efficiency at 24 h) was achieved by MSPP-ODN within 20 min. Moreover, when the magnetofection time was increased from 20 min to 1 h, only limited improvements on uptake efficiency were observed. The uptake efficiencies obtained from MSPP-ODN were about the same level as those obtained from MPP-ODN, which required 24 h for MSPP-ODN through non-magnetofection. Extended magnetofection time from 1 h to 24 h did not lead to a significant increase of uptake efficiency for MSPP-ODN, suggesting almost all MSPP-ODN had been taken up by cells within 1 h of magnetofection. This result demonstrated that MSPPs were capable of rapidly delivering ODNs into cells through magnetofection.

The uptake kinetics of MDA-MB-231 cells treated with SPP90-ODN was also investigated. As shown in Fig. 7d. No significant differences on uptake efficiencies were observed for cells incubated with SPP90-ODN with or without magnetic field, suggesting a magnetic field had no effect to the performance of SPPs. After 5 and 20 min of transfection time, lower uptake efficiencies were observed for cells treated with SPP90-ODN (49%, 20 min) compared with MSPP90-ODN (51%, 20 min) when there was no magnetic field provided. However, slightly higher uptake efficiencies were obtained by SPP90-ODN (69%, 1 h) than MSPP90-ODN (65%, 1 h) when the transfection time was extended to 1 h or over. This can be attributed to more PEI in SPP90 than that in MSPP90 with the same overall weight, therefore facilitating the internalization over time.

3.4.2. Concentration effect on the uptake efficiency of MSPP90-ODN and SPP90-ODN on MDA-MB-231 cells and HDF cells

The ODN uptake efficiency for MDA-MB-231 is shown in Fig. 8a. Cells were incubated with naked ODNs and complexes at different

concentrations for 20 min before washed and further incubated for a final duration of 24 h. Fig. 8a clearly shows that increasing the concentration of MSPP90-ODN and SPP90-ODN lead to the improved uptake efficiencies for MDA-MB-231 cells, which explains why increased concentrations of transfection complexes resulted in decreased viability of cells as shown previously in Section 3.3.2. The uptake efficiencies obtained by Oligofectamine-ODN were 2.7, 5.7 and 3.7-fold higher than those obtained by naked ODNs at the concentration [C], 5[C] and 10[C] respectively, suggesting an enhanced uptake efficiency can be achieved by Oligofectamine within a short transfection time of 20 min. However, higher uptake efficiencies were obtained by MSPP90-ODN and SPP90-ODN with or without the presence of a magnetic field. In particular, with a magnetic field the uptake efficiency of MSPP90-ODN is much higher. The uptake efficiencies by HDFs, as a control of non-cancer cells, are displayed in Fig. 8b and are significantly lower than that of MDA-MB-231 breast cancer cells. These results explain why both MSPP90-ODN and SPP90-ODN exhibited a lower growth inhibition effect to HDF cells compared with MDA-MB-231 cells (see Section 3.3.2).

3.5. Magnetically targeted delivery assay

To investigate the potential of MSPPs for magnetically targeted delivery of ODNs, MSPP90-ODN were incubated with MDA-MB-231 cells with or without the presence of a magnet. Naked ODNs, Oligofectamine-ODN and SPP90-ODN were also incubated with cells as negative controls. As shown in Fig. 9a&b, fluorescence intensities of cells treated with naked ODNs were seen to be significantly lower than those cells treated with transfection complexes, suggesting naked ODNs were not efficiently internalized by cells, which is consistent with uptake efficiency shown in Fig. 7. Moreover, for cells treated with naked ODNs (Fig. 9a&b), Oligofectamine-ODN (Fig. 9c&d) and SPP90-ODN (Fig. 9e&f), the presence of the magnet did not result in any significant difference to the fluorescence intensities, suggesting that the magnetic field did not change the cellular uptake of these complexes. Fig. 9g&h reveals the uptake of MSPP90-ODN without and with a magnet placed under the cells respectively. With the presence of the magnet the ODN uptake was significantly enhanced. The improved ODN uptake is because large amounts of MSPP90-ODN were concentrated at the area with a magnet. On the other hand, the local concentration of MSPP90-ODN at the areas without magnet was significantly reduced, thus resulting in a reduced uptake. This result reveals that MSPPs have great potential to be used for magnetically targeted delivery of ODNs to desired sites.

4. Conclusions

In summary, magnetic-silk/polyethyleneimine core–shell nanoparticles have been fabricated using SF, PEI and MNPs through a simple salting-out method. The particle size and zeta potential are controllable by changing the percentage of SF during fabrication. The core–shell nanoparticles are capable of delivering ODNs into MDA-MB-231 breast cancer cells and significantly inhibiting cell growth. The addition of SF material resulted in significantly reduced cytotoxicity compared to MPPs. Both SPPs and MSPPs are less toxic to HDF cells than to MDA-MB-231 cancer cells. High uptake efficiency of ODNs (over 70%) was achieved by MSPPs within a short time (20 min) through magnetofection. Moreover, with the presence of external magnetic fields, MSPPs can target deliver ODNs to the desired areas with reduced ODN concentrations at non-targeting areas, thus avoiding undesirable side-effects to healthy tissue. SPPs and MSPPs therefore are promising candidates for targeted gene therapy.

Declaration of interest statement

The authors declare that there is no conflict of interest regarding the

publication of this article.

Acknowledgements

References

Andrushchenko, V., Leonenko, Z., Cramb, D., van de Sande, H., Wieser, H., 2002. Vibrational CD (VCD) and atomic force microscopy (AFM) study of DNA interaction with Cr3+ ions: VCD and AFM evidence of DNA condensation. Biopolymers 61 (4), 243–260. https://doi.org/10.1002/bip.10159.

Arscott, P.G., Li, A.Z., Bloomfield, V.A., 1990. Condensation of DNA by trivalent cations. 1. Effects of DNA length and topology on the size and shape of condensed particles. Biopolymers 30 (5–6), 619–630. https://doi.org/10.1002/bip.360300514.

Balaji, K., Koul, H., Mitra, S., Maramag, C., Reddy, P., Menon, M., Malhotra, R.K., Laxmanan, S., 1997. Antiproliferative effects of c-myc antisense oligonucleotide in prostate cancer cells: a novel therapy in prostate cancer. J. Urol. 50 (6), 1007–1015. https://doi.org/10.1016/S0090-4295(97)00390-7.

Bansal, R., Kiran, P., Kumar, P., 2016. Synthesis, characterization and evaluation of di-glycidyl-1, 2-cyclohexanedicarboxylate crosslinked polyethylenimine nanoparticles as efficient carriers of DNA. New J. Chem. 40 (6), 5044–5052. https://doi.org/10.1039/C5NJ02953H.

Chandler, D., 2005. Interfaces and the driving force of hydrophobic assembly. Nature 437 (7059), 640–647. https://doi.org/10.1038/nature04162.

Chaves, N.L., Estrela-Lopis, I., Böttner, J., Lopes, C.A., Guido, B.C., de Sousa, A.R., Báo, S.N., 2017. Exploring cellular uptake of iron oxide nanoparticles associated with rhodium citrate in breast cancer cells. Int. J. Nanomed. 12, 5511–5523. https://doi.org/10.2147/IJN.S141582.

Chen, A.M., Santhakumaran, L.M., Nair, S.K., Amenta, P.S., Thomas, T., He, H., Thomas, T., 2006. Oligodeoxynucleotide nanostructure formation in the presence of poly-propyleneimine dendrimers and their uptake in breast cancer cells. Nanotechnology 17 (21), 5449–5460. https://doi.org/10.1088/0957-4484/17/21/027.

Chiorcea-Paquim, A.-M., Santos, P.V., Oliveira-Brett, A.M., 2013. Atomic force micro-scopy and voltammetric characterisation of synthetic homo-oligodeoxynucleotides. Electrochim. Acta 110, 599–607. https://doi.org/10.1016/j.electacta.2013.03.103.

Chiorcea-Paquim, A.-M., Santos, P.V., Eritja, R., Oliveira-Brett, A.M., 2013. Self-as-sembled G-quadruplex nanostructures: AFM and voltammetric characterization. Phys. Chem. Chem. Phys. 15 (23), 9117–9124. https://doi.org/10.1039/C3CP50866H.

Costa, I., Kerkmann, M., Hartmann, G., Endres, S., Bisch, P., Heckl, W., Thalhammer, S., 2004. Structural studies of oligonucleotides containing G-quadruplex motifs using AFM. Biochem. Biophys. Res. Commun. 313 (4), 1065–1072. https://doi.org/10.1016/j.bbrc.2003.12.041.

Curtis, K.A., Miller, D., Millard, P., Basu, S., Horkay, F., Chandran, P.L., 2016. Unusual salt and pH induced changes in polyethylenimine solutions. PLoS One 11 (9), e0158147. https://doi.org/10.1371/journal.pone.0158147.

Dal Pra, I., Freddi, G., Minic, J., Chiarini, A., Armato, U., 2005. De novo engineering of reticular connective tissue in vivo by silk fibroin nonwoven materials. Biomaterials 26 (14), 1987–1999. https://doi.org/10.1016/j.biomaterials.2004.06.036.

Danielsen, S., Vårum, K.M., Stokke, B.T., 2004. Structural analysis of chitosan mediated DNA condensation by AFM: influence of chitosan molecular parameters. Biomacromolecules 5 (3), 928–936. https://doi.org/10.1021/bm034502r.

De Smedt, S., Remaut, K., Lucas, B., Braeckmans, K., Sanders, N., Demeester, J., 2005. Studying biophysical barriers to DNA delivery by advanced light microscopy. Adv. Drug Delivery Rev. 57 (1), 191–210. https://doi.org/10.1016/j.addr.2004.06.003.

Dey, D., Inayathullah, M., Lee, A.S., LeMieux, M.C., Zhang, X., Wu, Y., Nag, D., De Almeida, P.E., Han, L., Rajadas, J., 2011. Efficient gene delivery of primary human cells using peptide linked polyethylenimine polymer hybrid. Biomaterials 32 (20), 4647–4658. https://doi.org/10.1016/j.biomaterials.2011.03.016.

Dobrynin, A.V., Rubinstein, M., 1999. Hydrophobic polyelectrolytes. Macromolecules 32 (3), 915–922. https://doi.org/10.1021/ma981412j.

Du, J., Zhu, W., Yang, L., Wu, C., Lin, B., Wu, J., Jin, R., Shen, T., Ai, H., 2016. Reduction of polyethylenimine-coated iron oxide nanoparticles induced autophagy and cyto-toxicity by lactosylation. Regen. Biomater. 3 (4), 223–229. https://doi.org/10.1093/rb/rbw023.

El-Aneed, 2004. An overview of current delivery systems in cancer gene therapy. J. Control Release 94 (1), 1–14. https://doi.org/10.1016/j.jconrel.2003.09.013.

Forrest, M.L., Koerber, J.T., Pack, D.W., 2003. A degradable polyethylenimine derivative with low toxicity for highly efficient gene delivery. Bioconjug. Chem. 14 (5), 934–940. https://doi.org/10.1021/bc034014g.

Gal, N., Massalha, S., Samuely-Nafta, O., Weihs, D., 2015. Effects of particle uptake, encapsulation, and localization in cancer cells on intracellular applications. Med. Eng. Phys. 37 (5), 478–483. https://doi.org/10.1016/j.medengphy.2015.03.003.

Gangar, A., Fegan, A., Kumarapperuma, S.C., Huynh, P., Benyumov, A., Wagner, C.R., 2013. Targeted delivery of antisense oligonucleotides by chemically self-assembled nanostructures. Mol. Pharmaceutics 10 (9), 3514–3518. https://doi.org/10.1021/mp400164f.

Ghiamkazemi, S., Amanzadeh, A., Dinarvand, R., Rafiee-Tehrani, M., Amini, M., 2010. Synthesis, and characterization, and evaluation of cellular effects of the FOL-PEG-g-PEI-GAL nanoparticles as a potential non-viral vector for gene delivery. J.

Nanomater. 12, 5511–5523. https://doi.org/10.1155/2010/863136.

Gu, Y., Zhang, J., Ma, X., Kim, B.-W., Wang, H., Li, J., Pan, Y., Xu, Y., Ding, L., Yang, L., 2017. Stabilization of the c-Myc protein by CAMKIIγ promotes T cell lymphoma. Cancer Cell 32 (1), 115–128. https://doi.org/10.1016/j.ccell.2017.06.001. e7.

Hazan, R.B., Phillips, G.R., Qiao, R.F., Norton, L., Aaronson, S.A., 2000. Exogenous ex-pression of N-cadherin in breast cancer cells induces cell migration, invasion, and metastasis. J. Cell Biol. 148 (4), 779–790. https://doi.org/10.1083/jcb.148.4.779.

Horan, R.L., Antle, K., Collette, A.L., Wang, Y., Huang, J., Moreau, J.E., Volloch, V., Kaplan, D.L., Altman, G.H., 2005. In vitro degradation of silk fibroin. Biomaterials 26 (17), 3385–3393. https://doi.org/10.1016/j.biomaterials.2004.09.020.

Hoskins, C., Cuschieri, A., Wang, L., 2012. The cytotoxicity of polycationic iron oxide nanoparticles: common endpoint assays and alternative approaches for improved understanding of cellular response mechanism. J. Nanobiotechnol. 10 (1), 15. https://doi.org/10.1186/1477-3155-10-15.

Hoskins, C., Wang, L., Cheng, W.P., Cuschieri, A., 2012. Dilemmas in the reliable esti-mation of the in-vitro cell viability in magnetic nanoparticle engineering: which tests and what protocols? Nanoscale Res. Lett. 7 (1), 1–12. https://doi.org/10.1186/1556-276X-7-77.

Huth, S., Lausier, J., Gersting, S.W., Rudolph, C., Plank, C., Welsch, U., Rosenecker, J., 2004. Insights into the mechanism of magnetofection using PEI-based magnetofectins for gene transfer. J. Gene Med. 6 (8), 923–936. https://doi.org/10.1002/jgm.577.

Junghans, M., Kreuter, J., Zimmer, A., 2000. Antisense delivery using protamine–oligo-nucleotide particles. Nucleic Acids Res. 28 (10). https://doi.org/10.1093/nar/28.10.e45. e45–e45.

Kettler, K., Veltman, K., van de Meent, D., van Wezel, A., Hendriks, A.J., 2014. Cellular uptake of nanoparticles as determined by particle properties, experimental condi-tions, and cell type. Environ. Toxicol. Chem. 33 (3), 481–492. https://doi.org/10.1002/etc.2470.

Kohler, N., Sun, C., Wang, J., Zhang, M., 2005. Methotrexate-modified super-paramagnetic nanoparticles and their intracellular uptake into human cancer cells. Langmuir 21 (19), 8858–8864. https://doi.org/10.1021/la0503451.

Krötz, F., De Wit, C., Sohn, H.-Y., Zahler, S., Gloe, T., Pohl, U., Plank, C., 2003. Magnetofection—a highly efficient tool for antisense oligonucleotide delivery in vitro and in vivo. Mol. Ther. 7 (5), 700–710. https://doi.org/10.1016/S1525-0016(03)00065-0.

Lammel, A.S., Hu, X., Park, S.H., Kaplan, D.L., Scheibel, T.R., 2010. Controlling silk fi-broin particle features for drug delivery. Biomaterials 31 (16), 4583–4591. https://doi.org/10.1016/j.biomaterials.2010.02.024.

Leonetti, C., D'Agnano, I., Lozupone, F., Valentini, A., Geiser, T., Zon, G., Calabretta, B., Citro, G., Zupi, G., 1996. Antitumor effect of c-myc antisense phosphorothioate oli-godeoxynucleotides on human melanoma cells in vitro and in mice. JNCI 88 (7), 419–429. https://doi.org/10.1093/jnci/88.7.419.

Li, L., Puhl, S., Meinel, L., Germershaus, O., 2014. Silk fibroin layer-by-layer micro-capsules for localized gene delivery. Biomaterials 35 (27), 7929–7939. https://doi.org/10.1016/j.biomaterials.2014.05.062.

Liu, Y., You, R., Liu, G., Li, X., Sheng, W., Yang, J., Li, M., 2014. Antheraea pernyi silk fibroin-coated PEI/DNA complexes for targeted gene delivery in HEK 293 and HCT 116 cells. Int. J. Mol. Sci. 15 (5), 7049–7063. https://doi.org/10.3390/ijms15057049.

Lungwitz, U., Breunig, M., Blunk, T., Göpferich, A., 2005. Polyethylenimine-based non-viral gene delivery systems. Eur. J. Pharm. Biopharm. 60 (2), 247–266. https://doi.org/10.1016/j.ejpb.2004.11.011.

Luo, D., Saltzman, W.M., 2000. Enhancement of transfection by physical concentration of DNA at the cell surface. Nat. Biotechnol. 18 (8), 893–895. https://doi.org/10.1038/78523.

Ma, Y., Zhang, Z., Wang, X., Xia, W., Gu, H., 2011. Insights into the mechanism of magnetofection using MNPs-PEI/pDNA/free PEI magnetofectins. Int. J. Pharm. 419 (1), 247–254. https://doi.org/10.1016/j.ijpharm.2011.07.017.

Mathur, A.B., Gupta, V., 2010. Silk fibroin-derived nanoparticles for biomedical appli-cations. Nanomedicine 5 (5), 807–820. https://doi.org/10.2217/nnm.10.51.

McBain, S., Yiu, H., El Haj, A., Dobson, J., 2007. Polyethyleneimine functionalized iron oxide nanoparticles as agents for DNA delivery and transfection. J. Mater. Chem. 17 (24), 2561–2565. https://doi.org/10.1039/b617402g.

Mumcuoglu, D., Ekiz, M.S., Gunay, G., Tekinay, T., Tekinay, A.B., Guler, M.O., 2016. Cellular internalization of therapeutic oligonucleotides by peptide amphiphile na-nofibers and nanospheres. ACS Appl. Mater. Interfaces 8 (18), 11280–11287. https://doi.org/10.1021/acsami.6b01526.

Mykhaylyk, O., Antequera, Y.S., Vlaskou, D., Plank, C., 2007. Generation of magnetic nonviral gene transfer agents and magnetofection in vitro. Nat. Protoc. 2 (10), 2391–2411. https://doi.org/10.1038/nprot.2007.352.

Ono, M.Y., Spain, E.M., 1999. Dynamics of DNA condensates at the solid–liquid interface by atomic force microscopy. J. Am. Chem. Soc. 121 (32), 7330–7334. https://doi.org/10.1021/ja9915697.

Ota, S., Takahashi, Y., Tomitaka, A., Yamada, T., Kami, D., Watanabe, M., Takemura, Y., 2013. Transfection efficiency influenced by aggregation of DNA/polyethylenimine max/magnetic nanoparticle complexes. J. Nanopart. Res. 15 (5), 1–12. https://doi.org/10.1007/s11051-013-1653-y.

Pack, D.W., Hoffman, A.S., Pun, S., Stayton, P.S., 2005. Design and development of polymers for gene delivery. Nat. Rev. Drug Discov 4 (7), 581–593. https://doi.org/10.1038/nrd1775.

Pan, B., Cui, D., Sheng, Y., Ozkan, C., Gao, F., He, R., Li, Q., Xu, P., Huang, T., 2007. Dendrimer-modified magnetic nanoparticles enhance efficiency of gene delivery system. Cancer Res. 67 (17), 8156–8163. https://doi.org/10.1158/0008-5472.CAN-06-4762.

Pan, B., Cui, D., Xu, P., Ozkan, C., Feng, G., Ozkan, M., Huang, T., Chu, B., Li, Q., He, R., 2009. Synthesis and characterization of polyamidoamine dendrimer-coated multi-

walled carbon nanotubes and their application in gene delivery systems. Nanotechnology 20 (12), 125101–125109. https://doi.org/10.1088/0957-4484/20/12/125101.

Petrilli, R., Eloy, J.O., Marchetti, J.M., Lopez, R.F., Lee, R.J., 2014. Targeted lipid nanoparticles for antisense oligonucleotide delivery. Curr. Pharm. Biotechnol. 15 (9), 847–855. https://doi.org/10.2174/1389201015666141020155834.

Plank, C., Schillinger, U., Scherer, F., Bergemann, C., Rémy, J.-S., Krötz, F., Anton, M., Lausier, J., Rosenecker, J., 2003. The magnetofection method: using magnetic force to enhance gene delivery. J. Biol. Chem 384 (5), 737–747. https://doi.org/10.1515/BC.2003.082.

Santhakumaran, L.M., Thomas, T., Thomas, T., 2004. Enhanced cellular uptake of a triplex-forming oligonucleotide by nanoparticle formation in the presence of polypropylenimine dendrimers. Nucleic Acids Res. 32 (7), 2102–2112. https://doi.org/10.1093/nar/gkh526.

Sarkar, T., Conwell, C.C., Harvey, L.C., Santai, C.T., Hud, N.V., 2005. Condensation of oligonucleotides assembled into nicked and gapped duplexes: potential structures for oligonucleotide delivery. Nucleic Acids Res. 33 (1), 143–151. https://doi.org/10.1093/nar/gki156.

Scopes, R.K., 2013. Protein Purification: Principles and Practice. Springer Science & Business Media.

Seow, W.Y., Liang, K., Kurisawa, M., Hauser, C.A., 2013. Oxidation as a facile strategy to reduce the surface charge and toxicity of polyethyleneimine gene carriers. Biomacromolecules 14 (7), 2340–2346. https://doi.org/10.1021/bm4004628.

Smits, R., Koper, G., Mandel, M., 1993. The influence of nearest-and next-nearest-neighbor interactions on the potentiometric titration of linear poly (ethylenimine). J. Phys. Chem. 97 (21), 5745–5751. https://doi.org/10.1021/j100123a047.

Song, W., Muthana, M., Mukherjee, J., Falconer, R.J., Biggs, C.A., Zhao, X., 2017. Magnetic-silk core-shell nanoparticles as potential carriers for targeted delivery of curcumin into human breast cancer cells. ACS Biomater. Sci. Eng. 3 (6), 1027–1038. https://doi.org/10.1021/acsbiomaterials.7b00153.

Steitz, B., Hofmann, H., Kamau, S.W., Hassa, P.O., Hottiger, M.O., von Rechenberg, B., Hofmann-Amtenbrink, M., Petri-Fink, A., 2007. Characterization of PEI-coated superparamagnetic iron oxide nanoparticles for transfection: size distribution, colloidal properties and DNA interaction. J. Magn. Magn. Mater. 311 (1), 300–305. https://doi.org/10.1016/j.jmmm.2006.10.1194.

Strojan, K., Lojk, J., Bregar, V.B., Veranič, P., Pavlin, M., 2017. Glutathione reduces cytotoxicity of polyethyleneimine coated magnetic nanoparticles in CHO cells. Toxicol. In Vitro 41, 12–20. https://doi.org/10.1016/j.tiv.2017.02.007.

Vepari, C., Kaplan, D.L., 2007. Silk as a Biomaterial. Prog. Polym. Sci. 32 (8), 991–1007.

https://doi.org/10.1016/j.progpolymsci.2007.05.013.

Volcke, C., Pirotton, S., Grandfils, C., Humbert, C., Thiry, P., Ydens, I., Dubois, P., Raes, M., 2006. Influence of DNA condensation state on transfection efficiency in DNA/polymer complexes: an AFM and DLS comparative study. J. Biotechnol. 125 (1), 11–21. https://doi.org/10.1016/j.jbiotec.2006.02.010.

Wang, X., Zhou, L., Ma, Y., Li, X., Gu, H., 2009. Control of aggregate size of polyethyleneimine-coated magnetic nanoparticles for magnetofection. Nano Res. 2 (5), 365–372. https://doi.org/10.1007/s12274-009-9035-6.

Watson, P.H., Pon, R.T., Shiu, R.P., 1991. Inhibition of c-myc expression by phosphorothioate antisense oligonucleotide identifies a critical role for c-myc in the growth of human breast cancer. Cancer Res. 51 (15), 3996–4000.

Xiang, L., Bin, W., Huali, J., Wei, J., Jiesheng, T., Feng, G., Ying, L., 2007. Bacterial magnetic particles (BMPs)-PEI as a novel and efficient non-viral gene delivery system. J. Gene Med. 9 (8), 679–690. https://doi.org/10.1002/jgm.1068.

Xue, H.Y., Narvikar, M., Zhao, J.-B., Wong, H.L., 2013. Lipid encapsulation of cationic polymers in hybrid nanocarriers reduces their non-specific toxicity to breast epithelial cells. Pharm. Res. 30 (2), 572–583. https://doi.org/10.1007/s11095-012-0902-6.

Xue, H.Y., Liu, S., Wong, H.L., 2014. Nanotoxicity: a key obstacle to clinical translation of siRNA-based nanomedicine. Nanomedicine 9 (2), 295–312. https://doi.org/10.2217/nnm.13.204.

Yu, Y., Hu, Y., Li, X., Liu, Y., Li, M., Yang, J., Sheng, W., 2016. Spermine-modified Antheraea pernyi silk fibroin as a gene delivery carrier. Int. J. Nanomed. 11, 1013–1023. https://doi.org/10.2147/IJN.S82023.

Zhang, L., Li, Y., Jimmy, C.Y., Chen, Y.Y., Chan, K.M., 2014. Assembly of polyethylenimine-functionalized iron oxide nanoparticles as agents for DNA transfection with magnetofection technique. J. Mater. Chem. B 2 (45), 7936–7944. https://doi.org/10.1039/c4tb01577k.

Zhang, L., Li, Y., Jimmy, C.Y., Chan, K.M., 2016. Redox-responsive controlled DNA transfection and gene silencing based on polymer-conjugated magnetic nanoparticles. RSC Adv. 6 (76), 72155–72164. https://doi.org/10.1039/c6ra16578h.

Zhao, X., Pan, F., Zhang, Z., Grant, C., Ma, Y., Armes, S.P., Tang, Y., Lewis, A.L., Waigh, T., Lu, J.R., 2007. Nanostructure of polyplexes formed between cationic diblock copolymer and antisense oligodeoxynucleotide and its influence on cell transfection efficiency. Biomacromolecules 8 (11), 3493–3502. https://doi.org/10.1021/bm7006482.

Zhao, X., Cui, H., Chen, W., Wang, Y., Cui, B., Sun, C., Meng, Z., Liu, G., 2014. Morphology, structure and function characterization of PEI modified magnetic nanoparticles gene delivery system. PLoS One 9 (6), e98919. https://doi.org/10.1371/journal.pone.0098919.